Co-published by
Institute of Fluid-Flow Machinery
Polish Academy of Sciences
Committee on Thermodynamics and Combustion
Polish Academy of Sciences

Copyright©2024 by the Authors under licence CC BY-NC-ND 4.0

http://www.imp.gda.pl/archives-of-thermodynamics/

Evaluating the mixed convection flow of Casson fluid from the semi-infinite vertical plate with radiation absorption effect

Sonam, Rajendra Singh Yadav*

University of Rajasthan, Department of Mathematics, Jaipur, Rajasthan-302004, India
*Corresponding author email: rajendrauor@gmail.com

Received: 25.04.2024; revised: 19.06.2024; accepted:16.07.2024

Abstract

This study examines a steady laminar Casson fluid flow induced by a semi-infinite vertical plate under the impact of the Darcy-Forchheimer relation and thermal radiation. The features of mixed convection, cross-diffusion, radiation absorption, heat generation, chemical reactions and viscous dissipation are also considered to explain the transport phenomenon. The resultant system of equations, concerned with the problem under consideration, is transformed into a group of non-linear ordinary differential equations (ODEs) by means of similarity variables. The bvp4c method, an instrument popular for its numerical accomplishments, is utilized to solve this problem. The effect of flow parameters on heat transfer, concentration and velocity is evaluated via diagrams. To validate our code, we have compared the present outcomes to the prevenient literature, and stable consent has been detected. Moreover, the friction coefficient C_{f_x}, Nusselt number Nu_x, and Sherwood number Sh_x are also computed to assess velocity gradient, efficiency of heat transfer and mass transfer process, respectively.

Keywords: MHD flow; Radiation; Cross-diffusion; Slippiness; Chemical reactions

Vol. 45(2024), No. 4, 45–59; doi: 10.24425/ather.2024.151996

Cite this manuscript as: Sonam, & Yadav, R.S. (2024). Evaluating the mixed convection flow of Casson fluid from the semi-infinite vertical plate with radiation absorption effect. *Archives of Thermodynamics*, 45(4), 45–59.

1. Introduction

The review of non-Newtonian fluids has attracted a lot of interest due to their wide applications in manufacturing and industrial areas, particularly in polymer processing, the food industry to optimize sensory aspects, the oil and gas industry, and the formulation of beauty products. The Casson fluid, a shear-thinning fluid with lower resistance under high strain rates, is one variant of non-Newtonian fluids. Casson [1] was the one who first discovered it. Later, it was developed by Heller [2] to anticipate the flow properties of a pigment-oil mixture. Since then, the Casson fluid flow has been discussed by several scientists and researchers under various conditions. Ramana et al. [3] investigated the influence of the melting processes on Casson liquid. They noted that the large values of melting parameter decrease fluid concentration. The flow of electrically conducting Casson hybrid nanofluid along a vertical moving surface was pioneered by Krishna et al. [4]. Kodi et al. [5] have expounded on the heat and mass transfer of Casson fluid over the vertical plate. The study specifically accounted for the influence of heat absorption. Recently, Jaffrullah et al. [6] investigated the impacts of Joule heating and MHD (magnetohydrodynamics) on Casson fluid flow.

Nomenclature

B_0 – constant magnetic field, T
B_c – concentration slip parameter
B_t – temperature slip parameter
B_u – velocity slip parameter
c_p – specific heat at constant pressure, J kg^{-1}K^{-1}
c_s – species susceptibility, J kg^{-1}K^{-1}
C – fluid concentration, kg m^{-3}
C_b – drag force coefficient
C_{f_x} – local skin friction coefficient, N m^{-2}
C_w – wall concentration, kg m^{-3}
C_∞ – ambient concentration, kg m^{-3}
D_m – mass diffusivity factor, m^{2}s^{-1}
Du – Dufour number
Ec – Eckert number
f – dimensionless stream function
f' – dimensionless velocity
Fr – Forchheimer number
g – gravitational acceleration, m s^{-2}
Gm – concentration Grashof number
Gr – temperature Grashof number
K_0 – porous medium permeability, m^2
K_1 – porosity parameter
K_c – chemical reaction constant, s^{-1}
K_c' – chemical reaction parameter
K_T – thermal diffusion ratio, m^{2}s^{-1}
k^* – mean absorption coefficient, m^{-1}
L_0 – velocity slip factor, m
M – magnetic parameter
M_0 – thermal slip factor, m
N_0 – concentration slip factor, m
Nu_x – Nusselt number
Pr – Prandtl number
Q_0 – constant heat generation/absorption coefficient, W m^{-3}K^{-1}
Q^* – heat generation/absorption parameter
q_r – radiation heat flux, W m^{-2}
q_w – wall heat flux, W m^{-2}
R_0 – radiation absorption coefficient, W kg^{-1}
R^* – radiation absorption parameter
Re_x – Reynolds number
S – suction/blowing parameter
Sc – Schmidt number
Sr – Soret number
Sh_x – Sherwood number
T – temperature, K
T_m – mean temperature, K
T_w – wall temperature, K
T_∞ – ambient temperature, K
u, v – velocity components, m s^{-1}
v_0 – velocity suction/blowing, m s^{-1}
U_0 – velocity at wall, m s^{-1}
x, y – Cartesian coordinates, m

Greek Symbols

β_C – solute expansion coefficient, m^3 kg^{-1}
β_T – heat expansion coefficient, K^{-1}
γ – Casson parameter
θ – dimensionless temperature
η – similarity variable
k – thermal conductivity, W m^{-1}K^{-1}
μ – dynamic viscosity, Pa s
ρ – fluid density, kg m^{-3}
σ – electric conductivity, Ω^1 m^{-1}
σ^* – Stefan-Boltzmann coefficient, W m^{-2}K^{-4}
υ – viscosity, m^{2}s^{-1}
ψ – stream function. m^{2}s^{-1}
ϕ – dimensionless concentration

Subscripts and Superscripts

0 – condition at wall
w – condition at wall
∞ – ambient condition
' – differentiation with respect to η

Abbreviations and Acronyms

IVP – initial value problem
MHD – magnetohydrodynamics
ODE – ordinary differential equation
2D – two-dimensional

Fluids that exhibit boundary slippiness have numerous applications in tribology, influencing friction and reducing attrition in various mechanical systems such as engines and bearings. Furthermore, in the range of thermal exchangers, it significantly improves heat transfer efficiency across several industrial processes. Navier [7] initially came up with the concept of boundary slippiness. Later, Krishna and Chamkha [8] investigated the impact of slip on nanofluid flow from a vertical plate in the porous medium. Obalalu et al. [9] introduced the impact of velocity slip on the Casson nanofluid flow over a permeable surface. They noted a drop in velocity subject to large scales of slip parameters.

The theory of hydromagnetic flow has attracted a lot of sapidity in many industrial areas, particularly in the rate of cooling of ending materials [10]. The magnetic fields have also shown an appreciable interest in navigation systems, induction heating systems, MRI (magnetic resonance imaging) machines, and climate phenomenon management. Chamkha [11] deliberated on steady flow along a vertical plate under a magnetic field. Kumar et al. [12] have proposed the influence of magnetic fields on free convection fluid flow through porous sheets with chemical reactions. Lately, Raghunath et al. [13] have discussed MHD flow from an unbounded plate with radiation absorption. They reported a reversed effect on velocity subject to the magnetic parameter.

The phenomenon of fluid flow in porous media is utilized in many branches of engineering and applied sciences, particularly filtration, soil mechanics, petroleum engineering and water quality. The obtainable articles evidence that a lot of discussion has been stated about the problems of porous media that are developed by utilizing Darcy's theory. To forecast the effect of inertia, a quadratic term of velocity in the model of Darcian veloc-

ity is introduced by Forchheimer [14]. Aleem et al. [15] discussed the effects of chemical reactions and Newtonian heat on MHD nanofluids via Darcy medium. Nasir et al. [16] proposed a model by using Darcy-Forchheimer and entropy analysis effects on nanofluid.

The study of mixed convection flow plays a vital role in thermal engineering, especially in designing heating, cooling and ventilation systems for various applications. It is frequently found in extremely high-power output devices to dissipate all of the heat necessary. Bilal et al. [17] explored that the mixed convection of hybrid nanofluid increased the velocity profile. Sinha and Yadav [18] evaluated a numerical simulation of the convective slip flow over a porous plate. Roy et al. [19] focused on the transfer of heat via convection.

Engineering innovations like fluid gyroscopes and centrifuges involve suction and blowing, which is also in geophysics. In fact, chemical reactions use suction to eliminate reactor components [20]. On the contrary, blowing is applied to connect reactor components which chill planes and decrease drag [21]. Hussain et al. [22] have nicely explained the MHD flow of Williamson fluid with suction/blowing.

Chemical reactions have a major role in industrial processes due to their use in maximizing production and minimizing waste. Bejawada et al. [23] investigated the impact of radiation and chemical reactions on MHD Casson fluid flow over an inclined, non-linear surface. Raju et al. [24] analyzed the Soret impact on the water-based Jeffrey fluid flow from a semi-infinite vertical plate with chemical reactions and found an inverse behaviour of the reaction parameter on the concentration profile. Zhao et al. [25] had incurred chemical reactions in the flow of nanofluid to improve the concentration profile.

Thermal radiation is an essential concept in many engineering applications and significantly impacts the boundary layer flow due to its uses in technological and industrial fields such as polymer processing, re-entry vehicles, high-speed flights, furnace design and space technologies like aerodynamic rockets, propulsion systems, missiles, etc. Therefore, the effect of heat radiation cannot be disregarded. The word emission is widely used to signify the radiation of heat [26]. Asha and Sunitha [27] deliberated on the impact of radiation on peristaltic blood flow. In this literature, the approximation method (HAM – homotopy analysis method) is applied to explore the numerical solution. Later on, Abbas et al. [28] studied the Sakiadis flow with variable density and radiation impacts. Saravana et al. [29] analyzed the impact of radiation on fluid flow.

The phenomena of heat generation/absorption hold significant importance in various engineering and industrial processes, such as fertilization, filled-bed reactors, waste stowage materials and dissociating liquids. It is an essential characteristic of MHD Casson fluid flows. Gambo and Gambo [30] applied the influence of heat generation/absorption on fluid flow generated by a vertical annulus. This investigation took into account the existence of a magnetic field. Rao et al. [31] dealt with the effect of radiation absorption and heat sink/source on MHD free convective Casson fluid flow. They observed that the radiation absorption parameter adversely affects the Nusselt number. Thereafter, the idea of heat generation/absorption over ternary nanofluid flow was explored by Manjunatha et al. [32]. MHD heat transfer of Casson fluid over a moving wedge in the presence of internal heat generation/absorption impact is explored by Amar et al. [33].

The exploration of viscous dissipation and Joule heating has captured interest in their contribution to fluid flow and temperature distribution owing to their broad utility in many industrial and engineering applications [34]. These are the most significant thermal properties of fluid flow. Viscous dissipation is the modification of kinetic energy into heating energy under friction. Brinkman [35] initially came up with the concept of viscous dissipation. He also took into account the transportation of heat by convection. Later, Swain et al. [36] discussed the MHD flow of non-Newtonian fluid through a stretching sheet in the presence of viscous dissipation. They noted that the large values of the viscous parameter helped to raise the temperature. Das [37] observed the impacts of Joule heating and viscous dissipation on the Casson fluid's MHD convective slip flow over the inclined plate with thermal radiation. Sadia et al. [38] numerically analyzed the impact of Joule heating on the flow of Jeffrey fluid.

Thermo-diffusion, also known as thermophoresis or the Soret impact [39], is a phenomenon where particles migrate in a fluid through the interaction between the temperature and concentration gradients. It has applications in various fields such as heat transfer, particle separation and colloidal science. The diffusion-thermo or the Dufour effect [40] is the mutual phenomenon of thermo-diffusion. The presence of the Dufour effect is crucial in binary gas mixtures. A theoretical discussion of heat transfer on absorption kinetics with thermo-diffusion impact is explored by Krenn et al. [41]. The flow behaviour of hybrid nanofluid between two parallel plates was studied by Revathi et al. [42], with a specific focus on the impact of cross-diffusion. An increase in temperature is observed with an increasing Dufour number in this literature. Lately, Ullah et al. [43] conducted a study to explore the effect of cross-diffusion on Jeffery-Hamel flow in a stretching channel with Joule heating.

In sight of the extant literature, which primarily focuses on the discussions of steady flow of Casson fluid under different features [44–46], there is a notable gap in research regarding the examination of the combined impact of chemical reaction, radiation absorption, slip and heat source/sink on flow and heat transfer over a semi-infinite vertical plate in Darcy porous medium. This is the novelty of the present study. Inspired by this identified research gap, our goal is to yield a more elaborate understanding of the complex interplay between flow patterns and heat transfer conductors by incorporating these complex factors. The insights gained from this comprehensive analysis hold significance in various industrial processes like filtration, the food industry, climate phenomenon management, furnace design, and so forth. It can also aid our understanding of heat transfer in renewable energy systems.

2. Mathematical formulation

In order to construct our problem, we have made the following assumptions:

- The electrically conducting, non-compressible Casson fluid over a semi-infinite vertical plate in a Darcy porous medium is deemed.
- The plate is deemed to be along the vertical axis, i.e. the x-axis.
- The flow is regarded as steady, 2D, radiative, laminar, and mixed convective.
- T_w and C_w are the temperature and concentration at the plate, respectively.
- B_0 is the constant magnetic field employed at a right angle to the flow axis.
- In order to disregard the Hall impact and the propelled magnetic field, the magnetic Reynolds number is assumed to be low [47,48].
- T_∞ and C_∞ are the ambient temperature and mass, respectively.

The flow problem sketch is displayed in Fig. 1.

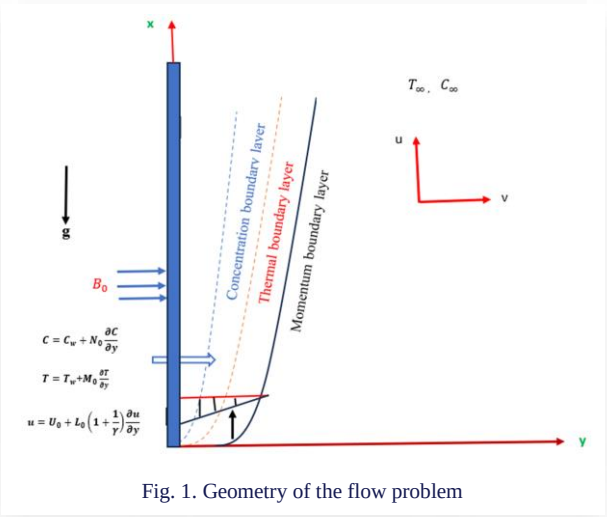

Fig. 1. Geometry of the flow problem

The rheological formula [3] for the Casson fluid model is:

$$\tau_{ij} = \begin{cases} 2\left(\mu_b + \frac{p_y}{\sqrt{2\pi}}\right)e_{ij}, & \pi > \pi_c, \\ 2\left(\mu_b + \frac{p_y}{\sqrt{2\pi_c}}\right)e_{ij}, & \pi < \pi_c, \end{cases} \quad (1)$$

where: τ_{ij} – $(i, j)^{th}$ component of the stress tensor, μ_b – plastic dynamic viscosity of the fluid, p_y – yield stress of the fluid, e_{ij} – $(i, j)^{th}$ component of the deformation rate, $\pi = e_{ij}e_{ij}$ – product of the component of deformation rate with itself, π_c – critical value of this product based on the non-Newtonian model.

To the impression as mentioned above, the modelling equations are described as follows [13,44,46]:

$$\frac{\partial u}{\partial x} + \frac{\partial v}{\partial y} = 0, \quad (2)$$

$$u\frac{\partial u}{\partial x} + v\frac{\partial u}{\partial y} = \frac{\mu}{\rho}\left(1+\frac{1}{\gamma}\right)\frac{\partial^2 u}{\partial y^2} - \frac{\sigma {B_0}^2}{\rho}u - \frac{\mu}{\rho K_0}u + \\ + g[\beta_T(T-T_\infty) + \beta_C(C-C_\infty)] - \frac{C_b}{\sqrt{K_0}}u^2, \quad (3)$$

$$\rho c_p\left(u\frac{\partial T}{\partial x} + v\frac{\partial T}{\partial y}\right) = k\frac{\partial^2 T}{\partial y^2} + \mu\left(1+\frac{1}{\gamma}\right)\left(\frac{\partial u}{\partial y}\right)^2 - \frac{\partial q_r}{\partial y} + \\ + \sigma {B_0}^2 u^2 + Q_0(T-T_\infty) + R_0(C-C_\infty) + \frac{\rho D_m K_T}{c_s}\frac{\partial^2 C}{\partial y^2}, \quad (4)$$

$$u\frac{\partial C}{\partial x} + v\frac{\partial C}{\partial y} = D_m\frac{\partial^2 C}{\partial y^2} + \frac{D_m K_T}{T_m}\frac{\partial^2 T}{\partial y^2} - K_c(C-C_\infty). \quad (5)$$

The associate boundary conditions:

$$\begin{cases} u = U_0 + L_0\left(1+\frac{1}{\gamma}\right)\frac{\partial u}{\partial y}, \ v = -v_0(x), \\ T = T_w + M_0\frac{\partial T}{\partial y}, \ C = C_w + N_0\frac{\partial C}{\partial y} \quad \text{at} \quad y = 0; \\ u \to 0, \ T \to T_\infty, \ C \to C_\infty \quad \text{as} \quad y \to \infty. \end{cases} \quad (6)$$

Here, u and v are the fluid speeds along x- and y-axes, respectively, c_s denotes the species susceptibility, K_T and K_c signifies the thermal-diffusion and constant of chemical reaction, respectively, heat expansion is expressed by β_T, μ, ρ are dynamic viscosity and liquid density, respectively, γ is the Casson parameter, K_0 is the porous medium permeability, q_r – heat fluctuation, C_b, β_C, D_m, T_m and σ stand for drag force factor, solute expression, mass diffusivity, mean temperature and fluid electric conductivity, respectively, R_0, Q_0, and c_p are the coefficients of radiation absorption, heat source/sink and specific heat, respectively, velocity suction/blowing is expressed by $v_0(x)$.

Incorporating the Rosseland approximation [49] for q_r as follows:

$$q_r = -\frac{4\sigma^*}{3k^*}\frac{\partial T^4}{\partial y}, \quad (7)$$

and extending the term T^4 in Taylor's expansion around T_∞ by ignoring high-order terms as

$$T^4 \cong 4T_\infty^3 T - 3T_\infty^4, \quad (8)$$

Eq. (4) can consequently be reformulated as

$$\rho c_p\left(u\frac{\partial T}{\partial x} + v\frac{\partial T}{\partial y}\right) = k\frac{\partial^2 T}{\partial y^2} + \sigma {B_0}^2 u^2 + \mu\left(1+\frac{1}{\gamma}\right)\left(\frac{\partial u}{\partial y}\right)^2 + \\ + \frac{16\sigma^* T_\infty^3}{3k^*}\frac{\partial^2 T}{\partial y^2} + Q_0(T-T_\infty) + R_0(C-C_\infty) + \frac{\rho D_m K_T}{c_s}\frac{\partial^2 C}{\partial y^2}. \quad (9)$$

Now, we introduce a dimensional variable η and functions $f(\eta), \theta(\eta)$, and $\phi(\eta)$ as follows:

$$\eta = \sqrt{\frac{U_0}{2\upsilon x}}\, y, \quad u = \frac{\partial \psi}{\partial y}, \quad v = -\frac{\partial \psi}{\partial x}, \quad \theta(\eta) = \frac{T-T_\infty}{T_w - T_\infty}, \\ \psi(x) = \sqrt{2\upsilon x U_0}\, f(\eta), \quad \phi(\eta) = \frac{C-C_\infty}{C_w - C_\infty}. \quad (10)$$

Enforcing Eq. (10) into Eqs. (3), (5), (6) and (9), we obtain the following set of ordinary differential equations (ODEs):

$$\left(1+\frac{1}{\gamma}\right)f''' + \mathrm{Gr}\,\theta - M\,f' - \mathrm{Fr}\,f'^2 + \mathrm{Gm}\,\phi + \\ - K_1 f' + f f'' = 0, \quad (11)$$

$$\frac{1}{\mathrm{Pr}}\left(1+\frac{4}{3}N\right)\theta'' + f\,\theta' + \mathrm{Du}\,\phi'' + \mathrm{Ec}\left(1+\frac{1}{\gamma}\right)f''^2 + \\ + \mathrm{Ec}\,M\,f'^2 + Q^*\theta + R^*\phi = 0, \quad (12)$$

$$\frac{1}{\mathrm{Sc}}\phi'' + \mathrm{Sr}\,\theta'' + f\,\phi' - K_c'\phi = 0, \quad (13)$$

and the boundary conditions:

$$f(0) = S, \quad f'(0) = 1 + \left(1 + \frac{1}{\gamma}\right) B_u f''(0),$$

$$\theta(0) = 1 + B_t \theta'(0), \quad \phi(0) = 1 + B_c \phi'(0) \text{ at } \eta = 0, \quad (14)$$

$$f' \to 0, \quad \theta \to 0, \quad \phi \to 0 \qquad \text{as } \eta \to \infty. \quad (15)$$

The relevant parameters are further specified as:

$\mathrm{Gr} = \frac{2g\beta_T x(T_w - T_\infty)}{{U_0}^2}$ – heat Grashof number, $N = \frac{4\sigma^* T_\infty^3}{k\,k^*}$ – radiation parameter, $\mathrm{Fr} = \frac{2C_b x}{\sqrt{K_0}}$ – Forchheimer number, $K_1 = \frac{2\upsilon x}{K_0 U_0}$ – porosity parameter, $\mathrm{Gm} = \frac{2g\beta_C x(C_w - C_\infty)}{{U_0}^2}$ – mass Grashof number, $M = \frac{2\sigma {B_0}^2 x}{U_0 \rho}$ – magnetic parameter, $\mathrm{Ec} = \frac{{U_0}^2}{c_p(T_w - T_\infty)}$ – Eckert number, $Q^* = \frac{2Q_0 x}{U_0 \rho c_p}$ – heat generation/absorption factor, $\mathrm{Pr} = \frac{\upsilon \rho C_p}{k}$ – Prandtl number, $\mathrm{Du} = \frac{D_m K_T}{\upsilon c_s c_p} \frac{(C_w - C_\infty)}{(T_w - T_\infty)}$ – Dufour number, $Sc = \frac{\upsilon}{D_m}$ – Schmidt number, $Sr = \frac{D_m K_T}{\upsilon T_m} \frac{(T_w - T_\infty)}{(C_w - C_\infty)}$ – Soret number, $R^* = \frac{2R_0 x}{U_0 \rho c_p} \frac{(C_w - C_\infty)}{(T_w - T_\infty)}$ – radiation absorption parameter, $K_c' = \frac{2K_c x}{U_0}$ – reaction parameter, $S = v_0 \sqrt{\frac{2x}{\upsilon U_0}}$ – suction (> 0)/blowing (< 0) parameter, $B_u = L_0 \sqrt{\frac{U_0}{2\upsilon x}}$ – velocity slip factor, $B_t = M_0 \sqrt{\frac{U_0}{2\upsilon x}}$ – thermal slip factor, and $B_c = N_0 \sqrt{\frac{U_0}{2\upsilon x}}$ – concentration slip factor.

Our concentration is now directed towards the examination of vital physical quantities, specifically skin-friction factor (C_{f_x}), Nusselt number (Nu_x) and Sherwood number (Sh_x). These paramount parameters play a fundamental role in deciphering flow dynamics and heat attributes. Their explicit formulations are presented below:

$$C_{f_x} = \frac{2\mu\left(1 + \frac{1}{\gamma}\right)\left(\frac{\partial u}{\partial y}\right)_{y=0}}{\rho {U_0}^2}, \quad (16)$$

$$\mathrm{Nu}_x = -\frac{x\left(k + \frac{16\sigma^* T_\infty^3}{3k^*}\right)\left(\frac{\partial T}{\partial y}\right)_{y=0}}{k(T_w - T_\infty)}, \quad (17)$$

$$\mathrm{Sh}_x = -\frac{x\left(\frac{\partial C}{\partial y}\right)_{y=0}}{(C_w - C_\infty)}. \quad (18)$$

Enforcing the similarity transformations given in Eq. (10), we get:

$$C_{f_x} = \frac{1}{\sqrt{\mathrm{Re}_x}}\left(1 + \frac{1}{\gamma}\right) f''(0), \quad (19)$$

$$\mathrm{Nu}_x = -\sqrt{\mathrm{Re}_x}\left(1 + \frac{4}{3}N\right)\theta'(0), \quad (20)$$

$$\mathrm{Sh}_x = -\sqrt{\mathrm{Re}_x}\phi'(0), \quad (21)$$

where $\mathrm{Re}_x = \frac{U_0 x}{2\upsilon}$ is the Reynolds number.

3. Numerical methodology

To evaluate the flow problem, the numerical technique bvp4c is exploited in MATLAB software. The initial step is to transmute the group of higher-order ODEs provided in Eqs. (11)–(13) and the boundary conditions in Eqs. (14)–(15) into an initial value problem (IPV) via a first-order process:

$$f = y_1, \; f' = y_2, \; f'' = y_3, \; \theta = y_4, \; \theta' = y_5,$$

$$\phi = y_6, \; \phi' = y_7,$$

$$y_3' = \left(\frac{1}{1 + \frac{1}{\gamma}}\right)(M\, y_2 + Fr\, {y_2}^2 + K_1\, y_2 - y_1\, y_3 + -Gr\, y_4 - Gm\, y_6). \quad (22)$$

$$y_5' = -\mathrm{Pr}\left\{\frac{\mathrm{Ec}\left[\left(1 + \frac{1}{\gamma}\right) {y_3}^2 + M\, {y_2}^2\right] + y_1\, y_5 + Q^*\, y_4 + R^*\, y_6 + \mathrm{DuSc}\,(K_c'\, y_6 - y_1\, y_7)}{\left(1 + \frac{4}{3}N - \mathrm{Pr}\,\mathrm{DuScSr}\right)}\right\}, \quad (23)$$

$$y_7' = -\mathrm{Sc}(y_1 y_7 + \mathrm{Sr} y_5' - K_c' y_6), \quad (24)$$

subject to:

$$\begin{cases} y_1(0) = S, \quad y_2(0) = 1 + \left(1 + \frac{1}{\gamma}\right) B_u\, y_3(0), \\ y_4(0) = 1 + B_t\, y_5(0), \quad y_6(0) = 1 + B_c\, y_7(0), \end{cases} \quad (25)$$

$$y_2 \to 0, \; y_4 \to 0, \; y_6 \to 0 \quad \text{as} \quad \eta \to \infty. \quad (26)$$

To provide a more precise estimate of the outcomes, the values of $y_3(0)$, $y_5(0)$ and $y_7(0)$ are improved with a maximum error of 10^{-5} and a step size of $h = 0.1$.

4. Validation of our code

In order to evaluate the precision of the proposed numerical technique, our results are compared with the outcomes achieved by

Table 1. Comparative analysis of C_{f_x}, Nu_x, and Sh_x with previous outcomes.

		Alam et al. [44]			Ram et al. [46]			Present result		
Sr	**Du**	C_{f_x}	Nu_x	Sh_x	C_{f_x}	Nu_x	Sh_x	C_{f_x}	Nu_x	Sh_x
2.0	0.030	6.2285	1.1565	0.1531	6.22686	1.15620	0.15352	6.2260	1.1561	0.1535
1.6	0.037	6.1491	1.1501	0.2283	6.14662	1.14971	0.22866	6.1466	1.1497	0.2287
1.2	0.050	6.0720	1.1428	0.3033	6.06948	1.14235	0.30358	6.0695	1.1423	0.3036
0.8	0.075	6.0006	1.1333	0.3781	5.99810	1.13285	0.37840	5.9981	1.1329	0.3784

Alam et al. [44] and Ram et al. [46]. The values of C_{f_x}, Nu_x and Sh_x are compared with the results of Alam et al. [44] and Ram et al. [46] for different levels of Sr and Du in Table 1 by taking $\mathrm{Sc} = 0.22$, $\mathrm{Pr} = 0.71$, $\mathrm{Gr} = 10$, $M = 0.3$, $\mathrm{Gm} = 4$, $S = 0.5$, $\mathrm{Fr} = K_c' = K_1 = Q^* = \mathrm{Ec} = N = R^* = B_u = B_t = B_c = 0$, $\gamma \to \infty$, $\mathrm{Re}_x = 1$. After making the comparisons, the bvp4c code was found to be precise and highly efficient.

5. Results and discussion

To figure out the physical understanding of the work, the numerical calculation is examined for various factors, and the possessed outcomes are manifested with the assistance of diagrams and tables. The context values in the existing study were chosen as $\gamma = 0.5$, $\mathrm{Gr} = 4$, $\mathrm{Gm} = M = \mathrm{Pr} = 2$, $N = 1.5$, $\mathrm{Sr} = \mathrm{Ec} = Q^* = 0.2$, $\mathrm{Du} = \mathrm{Sc} = 0.6$, $S = R^* = K_c' = 0.5$, $\mathrm{Fr} = K_1 = B_u = B_t = B_c = 1.0$, $\mathrm{Re}_x = 1$ and maintained fixed during the computations. Here,

- Schmidt number $\mathrm{Sc} = 0.6$, signifies water vapour;
- Prandtl number $\mathrm{Pr} = 2$, assents physically to water;
- Du and Sr are selected so that their multiplication is stable, and the mean temperature T_m remains stable as well;
- other values are selected at random.

The outcomes possessed from the numerical calculation are presented by figures displaying velocity $f'(\eta)$, temperature distribution $\theta(\eta)$ and concentration $\phi(\eta)$.

The change of the velocity amplitude $f'(\eta)$ for diverse Casson factor (γ) values is depicted in Fig. 2. Regarding that, an enhancement in γ decreases the flow rate magnitude. Because the augmentation in γ increases the yield stress, which bans the flow and molecules interplay, the substance develops a viscous bond. As a result, when γ increases, the flow rate decreases.

The effect of M on the velocity is verified in Fig. 3. It is explicit that velocity amplitude $f'(\eta)$ decreases with growth in M. The existence of magnetic induction in an electrically conducting liquid propels a protesting force named Lorentz force that

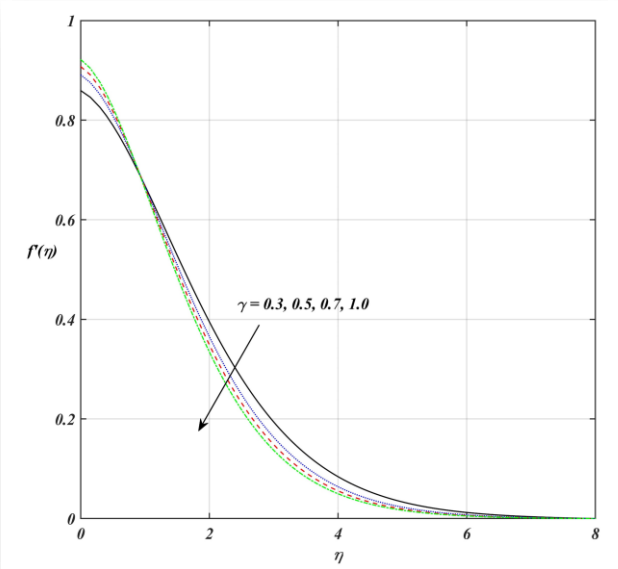

Fig. 2. The change of velocity with diverse values of γ.

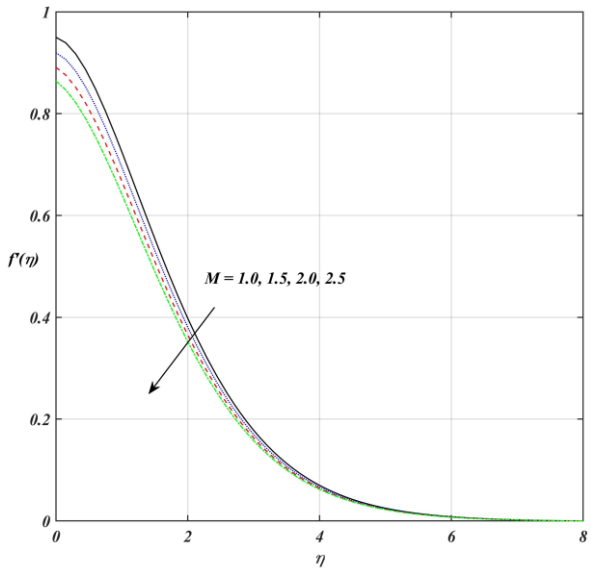

Fig. 3. The change of velocity with diverse values of M.

slows down the fluid motion. For the grater values of M, the Lorentz force becomes more apparent, leading to a damping in $f'(\eta)$. Conversely, the tiny values of M result in a significant augmentation in $f'(\eta)$. Hence, by adjusting the strength of the magnetic field, one can achieve the desired flow rate, which may be crucial for mechanical reasons when controlling fluid flow.

Figures 4 and 16 delineate the effect of S on dimensionless profiles $f'(\eta)$ and $\theta(\eta)$, respectively. It is noticed that suction $(S > 0)$ detracts flow rate and temperature phenomena, while blowing $(S < 0)$ augments them. This is because, suction $(S > 0)$ tends to thin the flake, while blowing $(S < 0)$ thickens it. This alteration in extent of the flake thickness influences fluid flow near the surface. Also, the thermal transmission rate (from the fluid to the surface) is slowed down. Thereby, suction or blowing can be used to control flow separation.

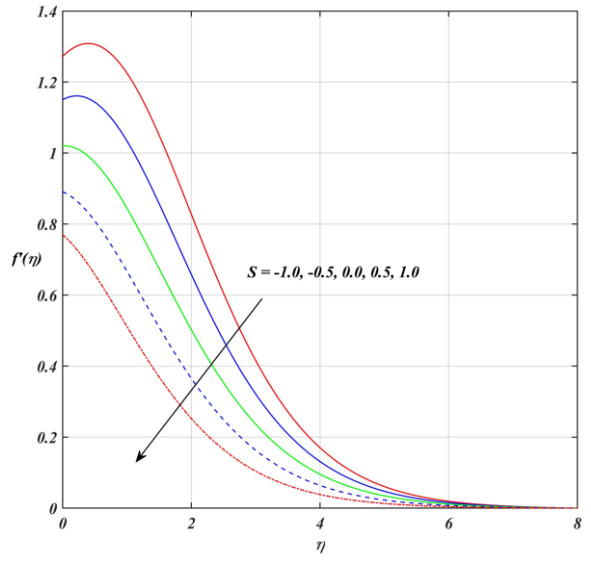

Fig. 4. The change of velocity with diverse values of S.

The change of the velocity amplitude $f'(\eta)$ for diverse values of heat (Gr) and mass (Gm) Grashof numbers is depicted in Figs. 5 and 6, respectively. It is manifested that a significant increase in surface refrigeration causes Gr and Gm to rise, resulting in an increase in velocity. Also, the growth in the value of Gr and Gm has the inclination to augment the thermal and mass buoyancy stress.

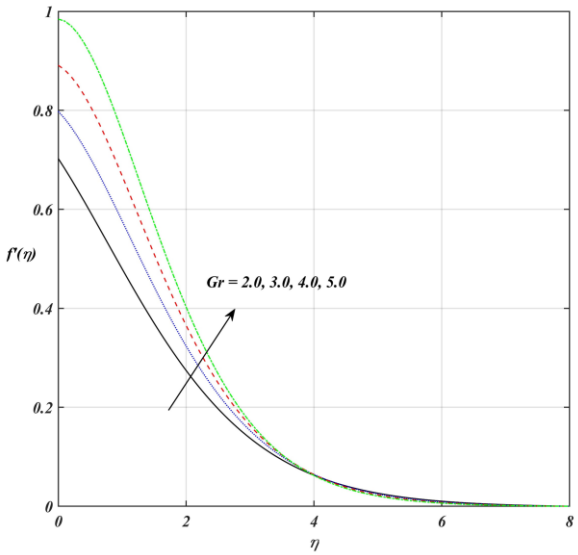

Fig. 5. The change of velocity with diverse values of Gr.

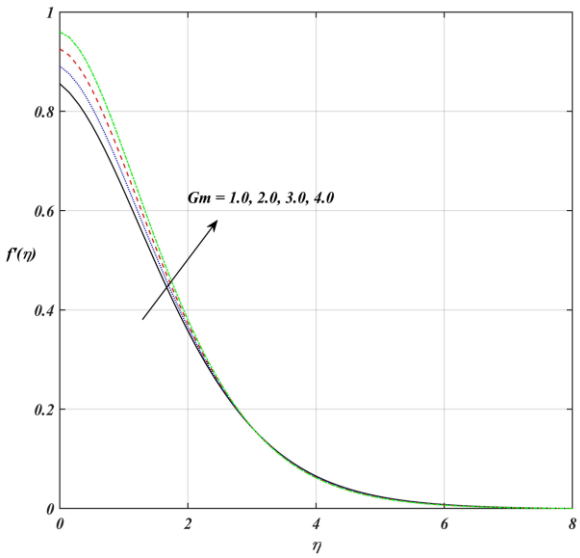

Fig. 6. The change of velocity with diverse values of Gm.

Figure 7 plots the behaviour of dimensionless profile $f'(\eta)$ with K_1. It should be noticed that the larger values of K_1 suggest a porous medium with low permeability and high dynamic viscosity as $K_1 = \frac{2\upsilon x}{K_0 U_0}$, which produces a higher fluid flow resistance. As seen in Fig. 7, rising values of K_1 result in a drop in $f'(\eta)$. Thus, the existence of porous media leads to a drop in flow velocity.

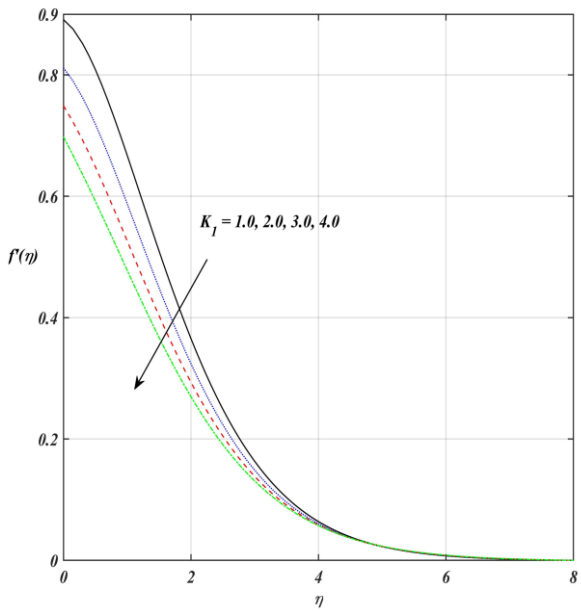

Fig. 7. The change of velocity with diverse values of K_1.

Figure 8 exhibits the effect of B_u on velocity profiles. Initially, the velocity decreases as B_u grows, but after $\eta = 1.5$, it slightly rises. This is because, as the slip stage happens, the velocity of the semi-infinite plate is not as analytic as the velocity of the flow near the plate.

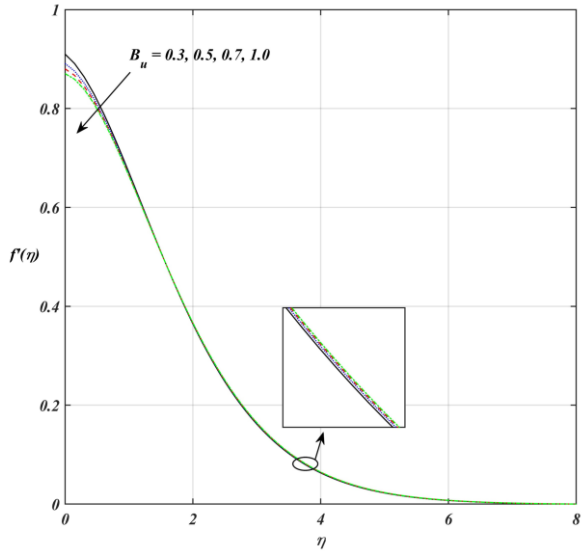

Fig. 8. The change of velocity with diverse values of B_u.

Figures 9 and 17 delineate the impressions of Dufour quantity Du on $f'(\eta)$ and $\theta(\eta)$, respectively. These profiles exhibit that $f'(\eta)$ and $\theta(\eta)$ both boost with rising values of Du. Physically, Du is the proportion of thermal diffusion and mass diffusion. For higher values of Du, thermal diffusion occurs much more effectively, and viscosity drops, leading to an augmentation in both $f'(\eta)$ and $\theta(\eta)$.

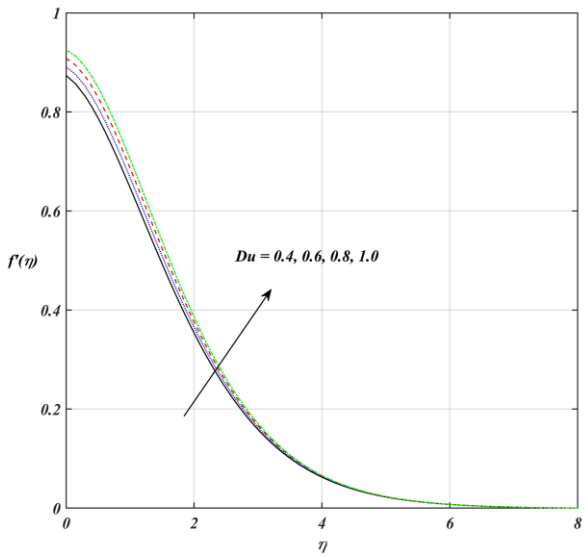

Fig. 9. The change of velocity with diverse values of Du.

Figure 10 declares the role of Fr on the momentum profile $f'(\eta)$. We detected that the momentum profile decreases as Fr rises, while it slightly increases away from the plate. Physically, grater values of Fr suggest a porous medium with low permeability and high dynamic viscosity as $\mathrm{Fr} = \frac{2C_b x}{\sqrt{K_0}}$, which produces a higher fluid flow resistance.

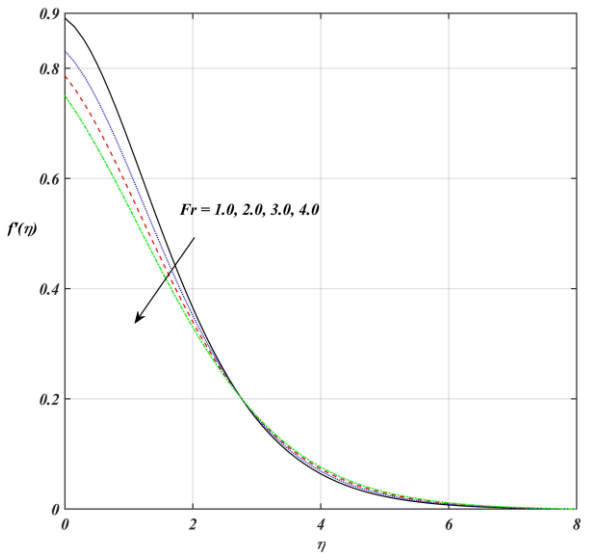

Fig. 10. The change of velocity with diverse values of Fr.

Figures 11 and 18 delineate the impressions of Ec on $f'(\eta)$ and $\theta(\eta)$, respectively. These profiles exhibit that velocity and temperature experience an increase with an increment in the dissipation parameter Ec. The existence of viscous dissipation causes the conversion of kinetic energy into internal energy as the fluid performs work against viscous forces. As a result, we may state that $f'(\eta)$ and $\theta(\eta)$ both are rising.

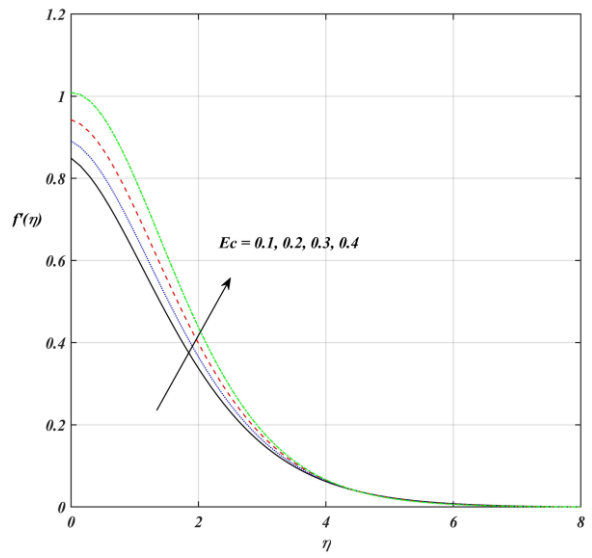

Fig. 11. The change of velocity with diverse values of Ec.

Figures 12 and 19 depict the responses of dimensionless profiles $f'(\eta)$ and $\theta(\eta)$ to diverse values of N within the boundary layer region, respectively. We detected that $f'(\eta)$ and $\theta(\eta)$ both rise as N increases. Physically, increasing values of N enhance the heat transfer performance from the plate to the fluid. Therefore, more heat is transmitted into the fluid for higher values of N. As a result, the surface temperature decreases, but the thermal boundary layer thickens.

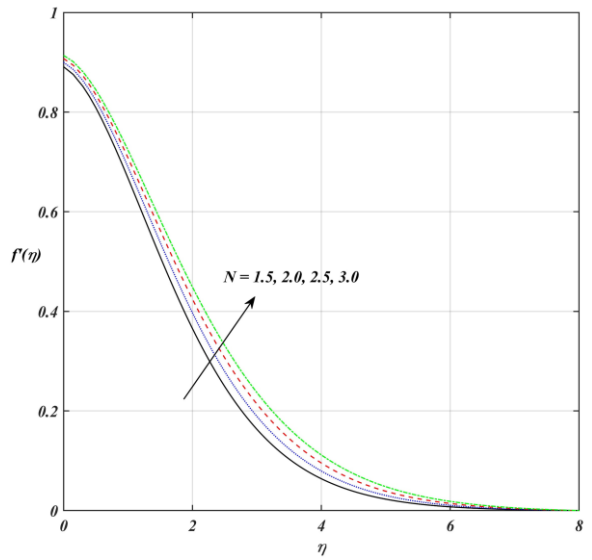

Fig. 12. The change of velocity with diverse values of N.

The change of the temperature $\theta(\eta)$ for diverse Casson factor (γ) values are depicted in Fig. 13. The yield stress or critical shear rate encourage molecular rigidity, which bans the liquid molecules from interplaying. In this context, when γ increases, the temperature distribution $\theta(\eta)$ decreases.

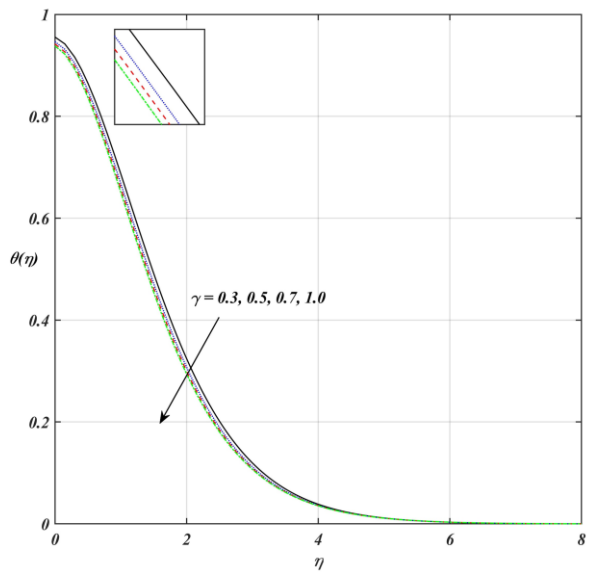

Fig. 13. The change of temperature with diverse values of γ.

Figure 14 is outlined to infer the effect of M on temperature. We found that the larger values of the magnetic parameter cause a rise in $\theta(\eta)$. This is because the higher values of the Lorentz force generate heat energy in flow, which promotes the increase of the thermal boundary layer.

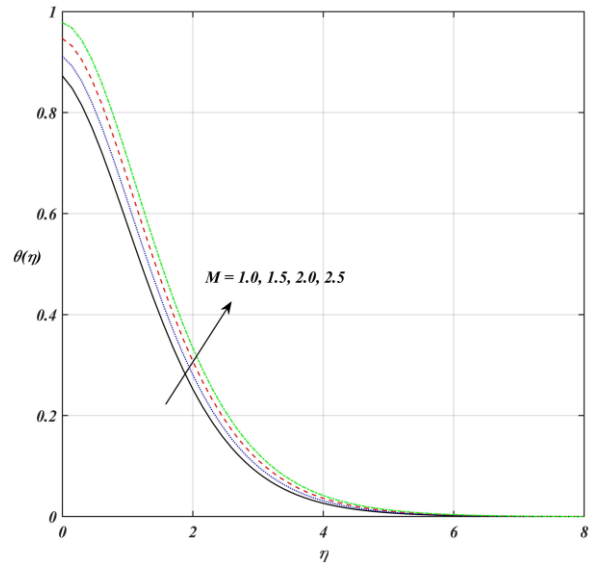

Fig. 14. The change of temperature with diverse values of M.

Figure 15 depicts the variation in dimensionless profile $\theta(\eta)$ for diverse values of Pr. It has been observed that fluid temperature reduces with enhanced Pr. This is due to the fact that the thermal conductivity of the substance is decreased with augmentation in Pr, resulting in a deficit in the thermal boundary layer. Additionally, Fig. 20 points out that the temperature $\theta(\eta)$ reduces as B_t rises because low heat is transported from the plate to the fluid.

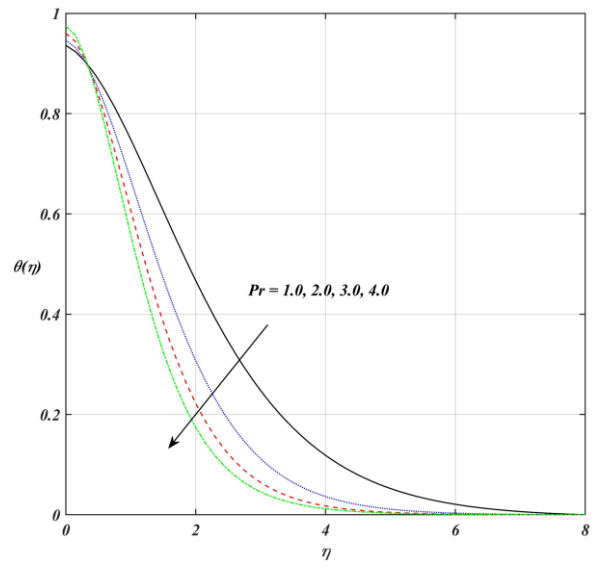

Fig. 15. The change of temperature with diverse values of Pr.

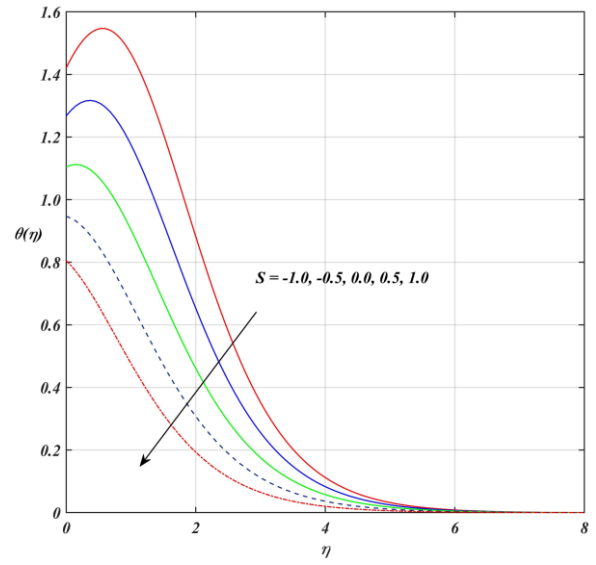

Fig. 16. The change of temperature with diverse values of S.

The effect of Q^* on $\theta(\eta)$ has been illustrated in Fig. 21. It indicates that heat transport is enhanced by internal heat generation ($Q^* > 0$). Consequently, the thermal boundary layer distends for greater values of Q^* (> 0). This phenomenon arises because an increase in the heat suction parameter amplifies the heat energy in the flow arrangement, thereby thickening the thermal boundary layer. It is also noted that increasing Q^* (> 0), causes a reduction in the heat transfer rate.

Figure 22 depicts the change of temperature $\theta(\eta)$ with varied values of R^*. It indicates that heat transport is enhanced by increasing values of R^* as heat is absorbed by the buoyancy accurate flow. Additionally, the thermal boundary layer thickness increases.

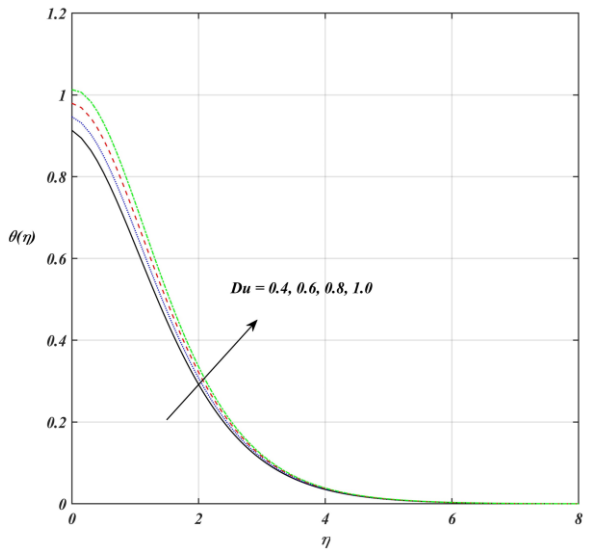

Fig. 17. The change of temperature with diverse values of Du.

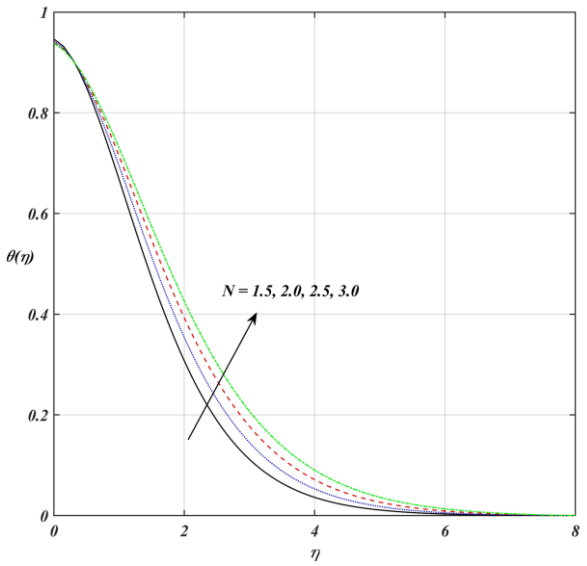

Fig. 19. The change of temperature with diverse values of N.

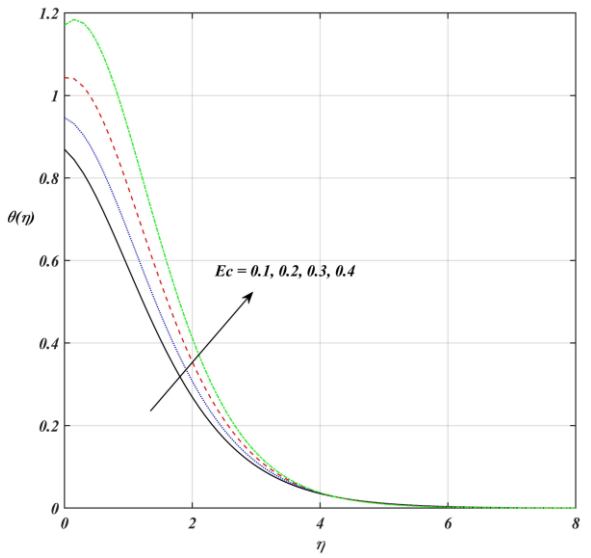

Fig. 18. The change of temperature with diverse values of Ec.

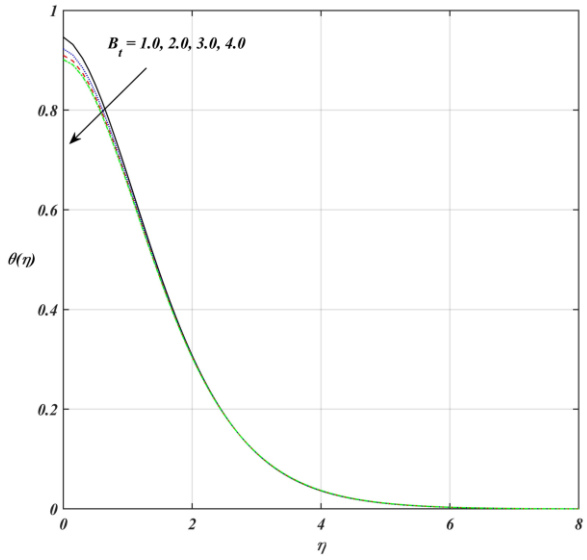

Fig. 20. The change of temperature with diverse values of B_t.

Figure 23 depicts the change of concentration $\phi(\eta)$ with different values of Sr. We detected that $\phi(\eta)$ is increased by augmentation of Sr. The impact of the Soret number is demonstrated by a dynamic molecule under the effect of temperature slope. This passes heavy molecules to a cold arrangement and slight molecules to a hot arrangement, which hereby leads to an enhanced concentration profile. Figure 24 portrays the change of concentration $\phi(\eta)$ with varied values of Sc. Physically, Sc is the proportion between kinematic viscosity and mass diffusivity, and the increment in mass diffusivity reduces Sc. So, the increasing trend in Sc reduces the species concentration. Additionally, Fig. 25 exhibits the effect of S on concentration $\phi(\eta)$. We detected that $\phi(\eta)$ is reduced by augmentation in S. This implies that the density of the concentration boundary layer decreases.

The effect of K_c' on concentration $\phi(\eta)$ is verified in Fig. 26. We explored that $\phi(\eta)$ diminishes as K_c' boosts. This is because as K_c' increases, the fluid becomes polarized, and the particles spread, decreasing the concentration of the fluid flow.

The change of C_{f_x} against K_1 for two values of M is shown in Fig. 27. It is observed that C_{f_x} reduces by raising both K_1 and M. Thus, the porous media with low permeability have a considerable role in enhancing the fluid flow resistance.

Figure 28 illustrates the tendency of Nu_x with the change of Pr for $\mathrm{Du} = 0.6, 1.0$. It is detected that Nu_x reduces by raising Pr and Du both. Moreover, Fig. 29 exhibits the behaviour of Sh_x against K_c' for two values of Sc. From this, it is noted that $\mathrm{Sh_x}$ grows with enhancing both K_c' and Sc.

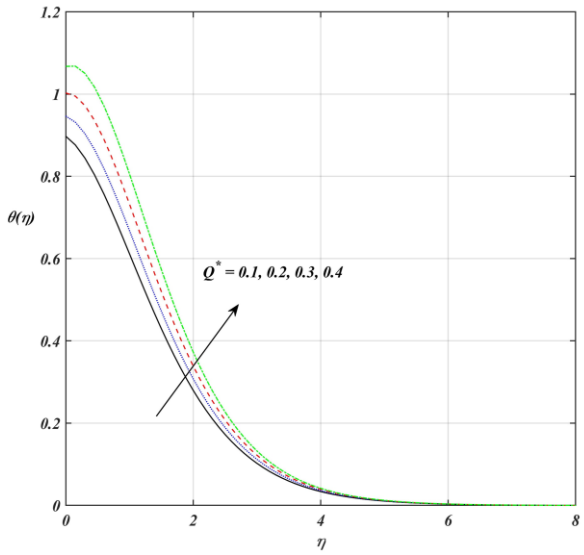

Fig. 21. The change of temperature with diverse values of Q^*.

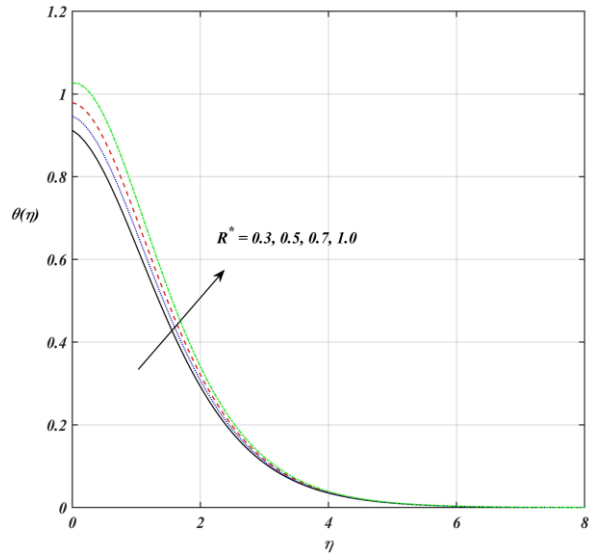

Fig. 22. The change of temperature with diverse values of R^*.

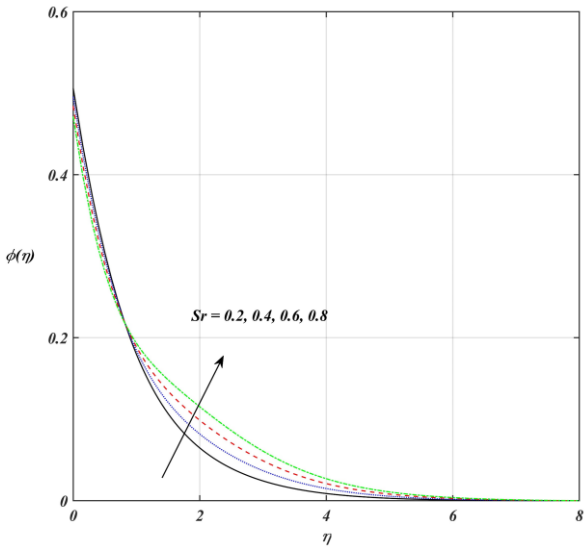

Fig. 23. The change of temperature with diverse values of Sr.

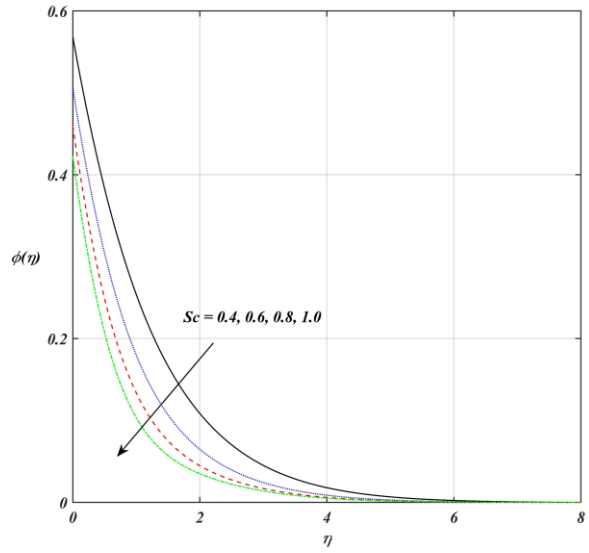

Fig. 24. The change of concentration with diverse values of Sc.

To comprehensively characterize the dynamics of flow and heat transfer, vital dimensionless physical quantities C_{f_x}, Nu_x and Sh_x are meticulously examined for varied governing parameters.

Tables 2 and 3 depict the reactions of C_{f_x} and Sh_x to varied values of governing parameters, respectively. A reduction in C_{f_x} is observed for enhancing values of M, Fr and K_1. Simultaneously, the Sherwood number Sh_x, another crucial quantity, exhibits a distinct pattern, i.e. it undergoes a notable escalation for increasing values of K_c', Sc and Sr.

In Table 4, we investigated how the parameters N, Q^*, R^*, and Du affect the Nusselt number Nu_x. It has been found that Nu_x decreases with an increase in the parameters Q^*, R^* and Du, while it grows under the influence of N.

Table 2. Data of C_{f_x} for varying levels of M, Fr, K_1 when $\mathrm{Re}_x = 1$.

M	Fr	K_1	C_{f_x}
1.0	1	1	-0.0998
1.5	1	1	-0.1606
2.0	1	1	-0.2178
2.0	1	1	-0.2178
2.0	2	1	-0.3367
2.0	3	1	-0.4268
2.0	1	1	-0.2178
2.0	1	2	-0.3764
2.0	1	3	-0.5016

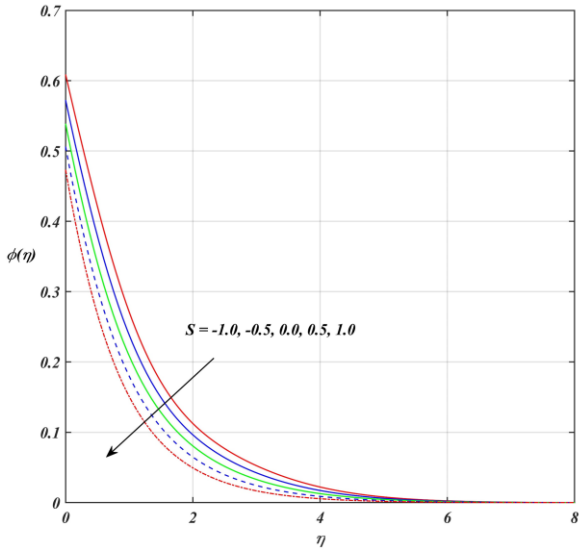

Fig. 25. The change of concentration with diverse values of S.

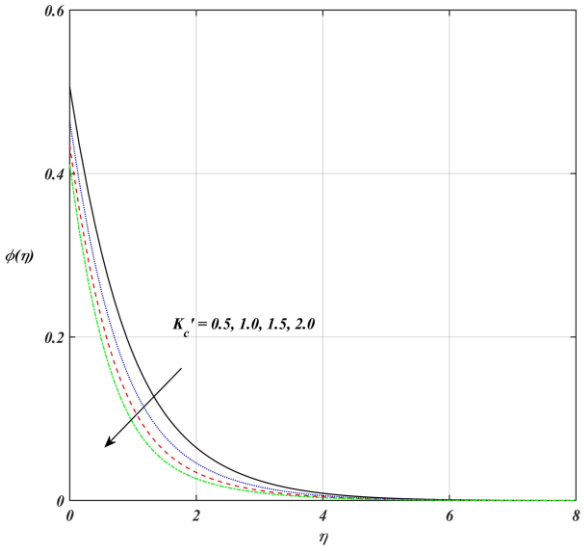

Fig. 26. The change of concentration with diverse values of K_c'.

Table 3. Data of Sh_x for several levels of $K_c', \mathrm{Sc}, \mathrm{Sr}$ when $\mathrm{Re}_x = 1$.

K_c'	Sc	Sr	Sh_x
0.5	0.6	0.2	0.4937
1.0	0.6	0.2	0.5348
1.5	0.6	0.2	0.5651
0.5	0.4	0.2	0.4314
2.0	0.6	0.2	0.4937
2.0	0.8	0.2	0.5402
2.0	0.6	0.2	0.4937
2.0	0.6	0.4	0.5042
2.0	0.6	0.6	0.5157

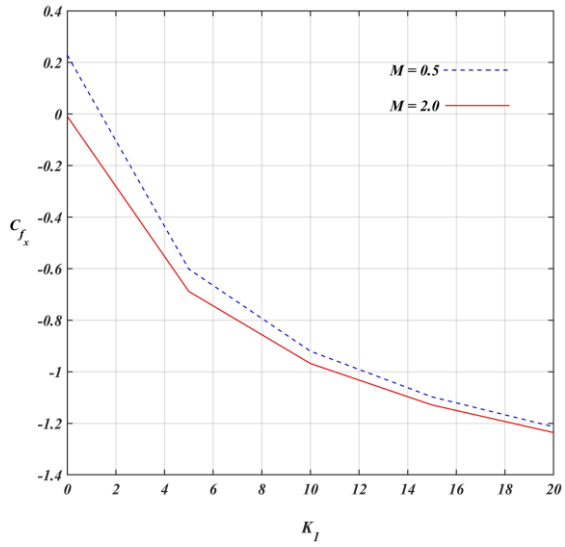

Fig. 27. Variance in C_{f_x} against K_1 and M.

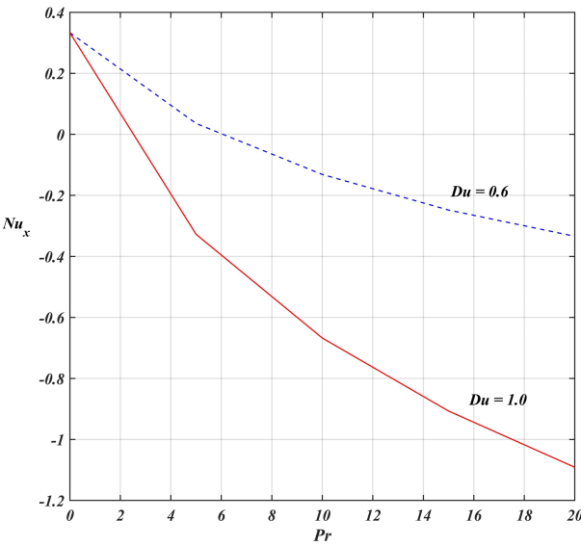

Fig. 28. Variance in Nu_x against Pr and Du.

Table 4. Data of Nu_x for different levels of N, Q^*, R^*, Du when $\mathrm{Re}_x = 1$.

N	Q^*	R^*	Du	Nu_x
1.5	0.2	0.5	0.6	0.1603
2.0	0.2	0.5	0.6	0.2116
2.5	0.2	0.5	0.6	0.2612
1.5	0.1	0.5	0.6	0.3073
1.5	0.2	0.5	0.6	0.1603
1.5	0.3	0.5	0.6	-0.0086
1.5	0.2	0.3	0.6	0.2627
1.5	0.2	0.5	0.6	0.1603
1.5	0.2	0.7	0.6	0.0617
1.5	0.2	0.5	0.4	0.2593
1.5	0.2	0.5	0.6	0.1603
1.5	0.2	0.5	0.8	0.0608

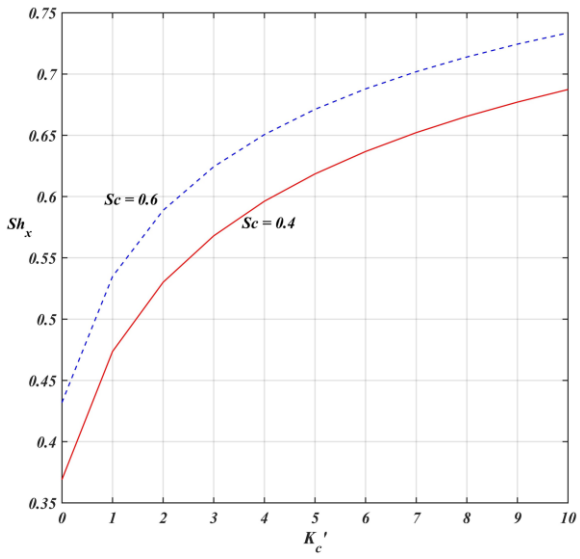

Fig. 29. Variance in Sh_x against K_c' and Sc.

6. Conclusions

In the current work, the influence of radiation absorption and viscous dissipation on the MHD mixed convection flow of Casson fluid from a semi-infinite vertical plate has been investigated mathematically. The governing equations were solved numerically employing an entirely inherent bvp4c method. The comparative interpretation was also noted pictorially. The effects of several physical parameters on $f'(\eta), \theta(\eta)$ and $\phi(\eta)$ are described as follows:

- Suction parameter $(S > 0)$ lowers the velocity, temperature and concentration profiles, while the effect of the blowing parameter $(S < 0)$ is reverse.
- An enhancement in the parameters N, Ec, and Du led to a rise in temperature and velocity, while the effect of the Casson parameter is opposite.
- A growth in the parameters K_1, B_u, M, and Fr led to a reduction in velocity, while the effect of Gr and Gm is reverse.
- A growth in the parameters $Q^*, R^*$and M led to an augmentation in temperature, while the effect of Pr and B_t is reverse.
- An increase in the reaction parameter and Schmidth number led to a reduction in the concentration profile, while the effect of the Soret number is opposite.
- The local skin friction decreased with improvements in magnetic parameter, Forchheimer number and porosity parameter.
- The local Nusselt number was reduced with an enhancement in Prandtl number, heat generation parameter, absorption parameter and Dufour number while increasing with the radiation parameter.
- The Sherwood number was enlarged with an enhancement in the Soret number, Schmidt number and reaction parameter.

Acknowledgements

This work was supported by Sonam by the CSIR- HRDG Ph.D. grant (09/149(0740)/2019-EMR-I), Ministry of Science & Technology, Government of India.

References

[1] Casson, N.A. (1959). A flow equation for the pigment-oil suspensions of the printing ink type. In: *Rheology of Disperse Systems* (C.C. Mill, ed.), (pp. 84–102). Pergamon Press.

[2] Heller, W. (1960b). Rheology of disperse systems, *Proceedings of a Conference Organized by the British Society of Rheology*, (C.C. MILL, ed.). Pergamon Press, New York, 1959, VII + 223. *Journal of Polymer Science*, 47(149), 537–538. doi: 10.1002/pol.1960.1204714975

[3] Ramana, R.M., Kumar, J.G., & Raju, K.V. (2020). Melting and radiation effects on MHD heat and mass transfer of Casson fluid flow past a permeable stretching sheet in the presence of chemical reaction. *AIP Conference Proceedings*, 2246(1), 020021. doi: 10.1063/5.0014732

[4] Krishna, M.V., Ahammad, N.A., & Chamkha, A.J. (2021). Radiative MHD flow of Casson hybrid nanofluid over an infinite exponentially accelerated vertical porous surface. *Case Studies in Thermal Engineering*, 27, 101229. doi: 10.1016/j.csite.2021.101229

[5] Kodi, R., Mopuri, O., Sree, S., & Konduru, V. (2021). Investigation of MHD Casson fluid flow past a vertical porous plate under the influence of thermal diffusion and chemical reaction. *Heat Transfer*, 51(1), 377–394. doi: 10.1002/htj.22311

[6] Jaffrullah, N.S., Sridhar, N.W., & Ganesh, N.G.R. (2023). MHD radiative Casson fluid flow through Forchheimer permeable medium with Joule heating influence. *CFD Letters*, 115(8), 79–199. doi: 10.37934/cfdl.15.8.179199

[7] Navier, H. (1827). Mémoire sur les lois du mouvement des fluides. *Mémoires de l'Académie des sciences de l'Institut de France*, 6.

[8] Krishna, M.V., & Chamkha, A.J. (2019). Hall and ion slip effects on MHD rotating boundary layer flow of nanofluid past an infinite vertical plate embedded in a porous medium. *Results in Physics*, 15, 102652. doi: 10.1016/j.rinp.2019.102652

[9] Obalalu, A.M., Ajala, O.A., Abdulraheem, A., & Akindele, A.O. (2021). The influence of variable electrical conductivity on non-Darcian Casson nanofluid flow with first and second-order slip conditions. *Partial Differential Equations in Applied Mathematics*, 4, 100084. doi: 10.1016/j.padiff.2021.100084

[10] Vajravelu, K., & Hadjinicolaou, A. (1997). Convective heat transfer in an electrically conducting fluid at a stretching surface with uniform free stream. *International Journal of Engineering Science*, 35(12–13), 1237–1244. doi: 10.1016/s0020-7225(97)00031-1

[11] Chamkha, A.J. (1999). Hydromagnetic three-dimensional free convection on a vertical stretching surface with heat generation or absorption. *International Journal of Heat and Fluid Flow*, 20(1), 84–92. doi: 10.1016/s0142-727x(98)10032-2

[12] Kumar, M.A., Reddy, Y.D., Goud, B.S., & Rao, V.S. (2022). An impact on non-Newtonian free convective MHD Casson fluid flow past a vertical porous plate in the existence of Soret, Dufour, and chemical reaction. *International Journal of Ambient Energy*, 43(1), 7410–7418. doi: 10.1080/01430750.2022. 2063381

[13] Raghunath, K., Obulesu, M., & Raju, K.V. (2023). Radiation absorption on MHD free conduction flow through porous medium over an unbounded vertical plate with heat source. *International*

Journal of Ambient Energy, 44(1), 1712–1720. doi: 10.1080/ 01430750.2023.2181869

[14] Forchheimer, P. (1901). *Wasserbewegung durch boden*. Zeitschrift des Vereins deutscher Ingenieure, 45, 1782–1788.

[15] Aleem, M., Asjad, M.I., Shaheen, A., & Khan, I. (2020). MHD influence on different water based nanofluids (TiO2, Al2O3, CuO) in porous medium with chemical reaction and Newtonian heating. *Chaos, Solitons & Fractals/Chaos, Solitons and Fractals*, 130, 109437. doi: 10.1016/j.chaos.2019.109437

[16] Nasir, S., Berrouk, A.S., Tassaddiq, A., Aamir, A., Akkurt, N., & Gul, T. (2023). Impact of entropy analysis and radiation on transportation of MHD advance nanofluid in porous surface using Darcy-Forchheimer model. *Chemical Physics Letters*, 811, 140221. doi: 10.1016/j.cplett.2022.140221

[17] Bilal, M., Khan, I., Gul, T., Tassaddiq, A., Alghamdi, W., Mukhtar, S., & Kumam, P. (2021). Darcy-Forchheimer hybrid nano fluid flow with mixed convection past an inclined cylinder. *Computers, Materials & Continua*, 66(2), 2025–2039. doi: 10.32604/cmc.2020.012677

[18] Sinha, S., & Yadav, R.S. (2022). MHD mixed convective slip flow along an inclined porous plate in presence of viscous dissipation and thermal radiation. *Trends in Sciences*, 19(4), 2685. doi: 10.48048/tis.2022.2685

[19] Roy, P.P., Chowdhury, S., Raj, M.H., Islam, M.Q., & Saha, S. (2023). Forced, natural and mixed convection of non-Newtonian fluid flows in a square chamber with moving lid and discrete bottom heating. *Results in Engineering*, 17, 100939. doi: 10.1016/ j.rineng.2023.100939

[20] Mukhopadhyay, S. (2009). Unsteady boundary layer flow and heat transfer past a porous stretching sheet in presence of variable viscosity and thermal diffusivity. *International Journal of Heat and Mass Transfer*, 52(21-22), 5213–5217. doi: 10.1016/ j.ijheatmasstransfer.2009.04.013

[21] Mukhopadhyay, S., & Vajravelu, K. (2012). Effects of transpiration and internal heat generation/absorption on the unsteady flow of a Maxwell fluid at a stretching surface. *Journal of Applied Mechanics*, 79(4), 044508. doi: 10.1115/1.4006260

[22] Hussain, M., Jahan, S., Ranjha, Q.A., Ahmad, J., Jamil, M.K., & Ali, A. (2022). Suction/blowing impact on magneto-hydrodynamic mixed convection flow of Williamson fluid through stretching porous wedge with viscous dissipation and internal heat generation/absorption. *Results in Engineering*, 16, 100709. doi: 10.1016/j.rineng.2022.100709

[23] Bejawada, S.G., Reddy, Y.D., Jamshed, W., Nisar, K.S., Alharbi, A.N., & Chouikh, R. (2022). Radiation effect on MHD Casson fluid flow over an inclined non-linear surface with chemical reaction in a Forchheimer porous medium. Alexandria Engineering Journal, 61(10), 8207–8220. doi: 10.1016/ j.aej.2022.01.043

[24] Raju, K.V., Mohanaramana, R., Reddy, S.S., & Raghunath, K. (2023). Chemical radiation and SoRET effects on unsteady MHD convective flow of Jeffrey nanofluid past an inclined semi-infinite vertical permeable moving plate. *Communications in Mathematics and Applications*, 14(1), 237–255. doi: 10.26713/cma. v14i1.1867

[25] Zhao, X., Mopuri, O., Raju, K. V., Farooq, S., Abdullaev, S., Alhazmi, H., Khan, S.U., & Jameel, M. (2024). Analysis of free convective flow of nanofluid due to inclined surface with thermos-diffusion effects and chemical reaction. *Tribology International*, 197, 109792. doi: 10.1016/j.triboint.2024.109792

[26] Planck, M. (1914). *The theory of heat radiation*. Blakiston.

[27] Asha, S., & Sunitha, G. (2020). Thermal radiation and Hall effects on peristaltic blood flow with double diffusion in the presence of nanoparticles. *Case Studies in Thermal Engineering*, 17, 100560. doi: 10.1016/j.csite.2019.100560

[28] Abbas, A., Ijaz, I., Ashraf, M., & Ahmad, H. (2021). Combined effects of variable density and thermal radiation on MHD Sakiadis flow. *Case Studies in Thermal Engineering*, 28, 101640. doi: 10.1016/j.csite.2021.101640

[29] Saravana, R., Reddy, R.H., Murthy, K.V.N., & Makinde, O.D. (2022). Thermal radiation and diffusion effects in MHD Williamson and Casson fluid flows past a slendering stretching surface. *Heat Transfer*, 51(4), 3187–3200. doi: 10.1002/htj.22443

[30] Gambo, J.J., & Gambo, D. (2020). On the effect of heat generation/absorption on magnetohydrodynamic free convective flow in a vertical annulus: An Adomian decomposition method. *Heat Transfer*, 50(3), 2288–2302. doi: 10.1002/htj.21978

[31] Rao, S.R., Vidyasagar, G., & Deekshitulu, G. (2021). Unsteady MHD free convection Casson fluid flow past an exponentially accelerated infinite vertical porous plate through porous medium in the presence of radiation absorption with heat generation/absorption. *Materials Today: Proceedings*, 42(3), 1608–1616. doi: 10.1016/j.matpr.2020.07.554

[32] Manjunatha, S., Puneeth, V., Gireesha, B., & Chamkha, A.J. (2022). theoretical study of convective heat transfer in ternary nanofluid flowing past a stretching sheet. *Journal of Applied and Computational Mechanics*, 8(4), 1279–1286. doi: 10.22055/ jacm.2021.37698.3067

[33] Amar, N., Kishan, N., & Goud, B.S. (2023). Viscous dissipation and radiation effects on MHD heat transfer flow of Casson fluid through a moving wedge with convective boundary condition in the existence of internal heat generation/absorption. *Journal of Nanofluids*, 12(3), 643–651. doi: 10.1166/jon.2023. 1948

[34] Ou, J.W., & Cheng, K.C. (1973). Viscous dissipation effects on thermal entrance region heat transfer in pipes with uniform wall heat flux. *Applied Scientific Research*, 28, 289–301. doi: 10.1007/ bf00413074

[35] Brinkman, H.C. (1951). Heat effects in capillary flow I. Applied Scientific Research. 2, 120– 124. doi: 10.1007/ bf00411976

[36] Swain, B., Parida, B., Kar, S., & Senapati, N. (2020). Viscous dissipation and Joule heating effect on MHD flow and heat transfer past a stretching sheet embedded in a porous medium. Heliyon, 6(10), e05338. doi: 10.1016/j.heliyon.2020.e05338

[37] Das, U.J. (2021). MHD mixed convective slip flow of Casson fluid over a porous inclined plate with Joule heating, viscous dissipation and thermal radiation. *Journal of Mathematical and Computational Science*, 11(3), 3263–3275. doi: 10.28919/jmcs/ 5713

[38] Sadia, H., Mustafa, M., & Farooq, M. (2023). Numerical and series solutions for von-Kármán flow of viscoelastic fluid inspired by viscous dissipation and Joule heating effects. *Alexandria Engineering Journal*, 75, 181–190. doi: 10.1016/j.aej. 2023.05.075

[39] Soret, C. (1880). Influence de la température sur la distribution des sels dans leurs solutions. *Comptes rendus de l'Académie des Sciences* (Paris), 91, 289.

[40] Dufour, L. (1872). The diffusion thermoeffect. *Archives des Sciences Physiques et Naturelles*, 45, 9–12.

[41] Krenn, P., Zimmermann, P., Fischlschweiger, M., & Zeiner, T. (2021). Influence of thermal diffusion on the solvent absorption kinetics of highly cross-linked epoxy resins. *Journal of Molecular Liquids*, 339, 116809. doi: 10.1016/j.molliq.2021.116809

[42] Revathi, G., Avadapu, S., Raju, C., Babu, M.J., Zidan, A., Alaoui, M.K., Shah, N.A., & Chung, J.D. (2023). Dynamics of Lorentz force and cross-diffusion effects on ethylene glycol-based hybrid nanofluid flow amidst two parallel plates with variable electrical conductivity: A multiple linear regression analysis. *Case Studies in Thermal Engineering*, 41, 102603. doi: 10.1016/j.csite.2022. 102603

[43] Ullah, S., Ullah, I., Ali, A., Shah, K., & Abdeljawad, T. (2024). Investigation of cross-diffusion effect on radiative Jeffery-Hamel flow in convergent/divergent stretchable channel with Lorentz force and Joule heating. *Alexandria Engineering Journal*, 86, 289–297. doi: 10.1016/j.aej.2023.11.054

[44] Alam, M.S., Ferdows, M., Ota, M., & Maleque, M.A. (2006). Dufour and Soret effects on steady free convection and mass transfer flow past a semi-infinite vertical porous plate in a porous medium. *International Journal of Applied Mechanics and Engineering*, 11(3), 535–545.

[45] Aruna, S., & Lakshmi, K.J. (2017). Combined effects of thermal diffusion and diffusion thermo on an unsteady MHD Casson fluid flow past a semi-infinite vertically inclined permeable moving plate. *Journal of Nanofluids*, 6(6), 1149–1159. doi: 10.1166/jon.2017.1403

[46] Ram, M.S., Ashok, N., & Shamshuddin, M.D. (2023). Numerical solution of radiative and dissipative flow on non-Newtonian Casson fluid model via infinite vertical plate with thermo-diffusion and diffusion-thermo effects. *Journal of Nanofluids*, 12(3), 777–785. doi: 10.1166/jon.2023.1976

[47] Krishna, M. V., Swarnalathamma, B., & Chamkha, A.J. (2019). Investigations of Soret, Joule and Hall effects on MHD rotating mixed convective flow past an infinite vertical porous plate. *Journal of Ocean Engineering and Science*, 4(3), 263–275. doi: 10.1016/j.joes.2019.05.002

[48] Kumar, B., Seth, G.S., Nandkeolyar, R., & Chamkha, A.J. (2019). Outlining the impact of induced magnetic field and thermal radiation on magneto-convection flow of dissipative fluid. *International Journal of Thermal Sciences*, 146, 106101. doi: 10.1016/j.ijthermalsci.2019.106101

[49] Brewster, M. Q. (1992). *Thermal radiative transfer and properties*. John Wiley & Sons.